Accepted Manuscript

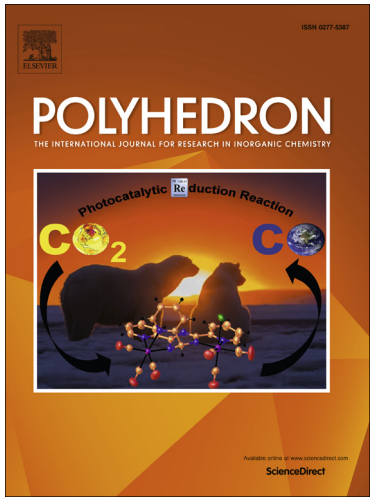

Syntheses and characterization of 2-acetylpyridine-aminoguanidine and its copper(II) complexes: Crystallographical and antimicrobial study

Ljiljana S. Vojinović-Ješić, Mirjana M. Radanović, Marko V. Rodić, Vukosava Živković-Radovanović, Ljiljana S. Jovanović, Vukadin M. Leovac

PII: S0277-5387(16)30266-2
DOI: http://dx.doi.org/10.1016/j.poly.2016.06.032
Reference: POLY 12073

To appear in: *Polyhedron*

Received Date: 13 March 2016
Accepted Date: 9 June 2016

Please cite this article as: L.S. Vojinović-Ješić, M.M. Radanović, M.V. Rodić, V. Živković-Radovanović, L.S. Jovanović, V.M. Leovac, Syntheses and characterization of 2-acetylpyridine-aminoguanidine and its copper(II) complexes: Crystallographical and antimicrobial study, *Polyhedron* (2016), doi: http://dx.doi.org/10.1016/j.poly.2016.06.032

Syntheses and characterization of 2-acetylpyridine-aminoguanidine and its copper(II) complexes: Crystallographical and antimicrobial study

Ljiljana S. Vojinović-Ješić[a], Mirjana M. Radanović[a], Marko V. Rodić[a], Vukosava Živković-Radovanović[b], Ljiljana S. Jovanović[a], Vukadin M. Leovac[a1]

[a] *Faculty of Sciences, University of Novi Sad, Trg Dositeja Obradovića 3, 21000 Novi Sad, Serbia*
[b] *Faculty of Chemistry, University of Belgrade, P.O. Box 51, 11158 Belgrade, Serbia*

Abstract

The syntheses, physico-chemical and microbiological properties of the ligand, 2-acetylpyridine-aminoguanidine dihydrogensulfate monohydrate and its five complexes with Cu(II) are described. The compounds were characterized by single crystal X-ray crystallography. Common fragments encountered in some of the structures were compared by r.m.s. overlay calculations as well as half-normal probability plots. In these complexes the chelate ligand is coordinated in its neutral form in a tridentate N_3-coordination mode, *via* pyridine, azomethine and imino nitrogen atoms of the aminoguanidine fragment. In these complexes the Cu(II) ion is situated in moderately or severely distorted square-pyramidal surroundings. The antimicrobial activity of the ligand and the complexes were examined against 6 selected bacterial and 3 fungal strains.

Keywords: 2-acetylpyridine-aminoguanidine, copper(II) complexes, crystal structure, spectra, antimicrobial activity

1. Introduction

During the last decade, many aromatic Schiff bases were widely investigated for their possible antimicrobial application due to their often prominent antibacterial and antiviral effects and some of those compounds showed promising antitumor activity [1-4]. Aminoguanidine is known as one of the most powerful inhibitors of carbonyl stress and the occurrence of diabetic complications [5-7]; hence, interest in the investigation of its Schiff bases with aromatic carbonyl compounds and their transition metal complexes has arisen [8-12].

A survey of Schiff bases of non-substituted and substituted aminoguanidine in the Cambridge Structural Database [13] revealed 77 structures with 54 different carbonyl compounds. However, the number of structurally characterized complexes with these Schiff bases is still small. The most numerous are complexes of copper(II) with pyridoxilidene aminoguanidine [14] and salicylidene aminoguanidine [12,15-17].

Bearing in mind the recognized biological importance of aminoguanidine and its Schiff bases, as well as their interesting coordination behavior, we found it important to examine the syntheses and characteristics of copper(II) complexes with the Schiff base of aminoguanidine and 2-acetylpyridine. Here we describe the syntheses, physicochemical,

[1] Corresponding author. E-mail address: vukadin.leovac@dh.uns.ac.rs (V.M. Leovac)

structural and antimicrobial properties of the ligand, 2-acetylpyridine-aminoguanidine dihydrogensulfate monohydrate and its Cu(II) complexes.

2. Experimental

2.1. Materials and physical measurements

All commercially obtained reagent-grade chemicals were used without further purification. The ligand 2-acetylpyridine-aminoguanidine dihydrogenchloride, L·2HCl, was prepared according to a previously described procedure [18] with a slight modification.

Elemental analyses (C, H, N and S) of the air-dried compounds were carried out by standard micro-methods in the Center for Instrumental Analyses, ICTN in Belgrade. The chlorine content was determined by potentiometric titration using $AgNO_3$. The compound was combusted using the Schoeniger method [19] and the products were absorbed in a solution of H_2O_2 and KOH. Molar conductivity measurements of freshly prepared 1 mM solutions were performed on a Jenway 4010 conductivity meter. IR spectra were recorded on a Nicolet Nexus 670 FTIR (Thermo Scientific) spectrophotometer in the range 400-4000 cm^{-1} by the KBr pellet technique. Electronic spectra of DMF solutions of the ligand and the complexes were recorded on a T80+UV-Vis spectrometer (PG Instruments, Ltd.), in the spectral range 270-1000 nm.

2.2. Syntheses

2.2.1. L·2HCl, 2-acetylpyridine-aminoguanidine dihydrogenchloride

Aminoguanidine-hydrogencarbonate (3.4 g, 25 mmol) was dissolved in 25 mL 2N HCl. After the addition of 2-acetylpyridine (2.8 mL, 25 mmol) the reaction mixture was heated for 1 h. The obtained microcrystalline product was evaporated nearly to dryness, using hot air, filtered in vacuo and washed with MeOH. Yield: 4.37 g (70%). Single crystals of the ligand were obtained by recrystallization from warm MeOH. Anal. Calc. for $C_8H_{13}N_5Cl_2$: C, 38.43; H, 5.20; N, 28.01; Cl, 28.34. Found: C, 38.10; H, 5.47; N, 27.76; Cl, 27.99%. Conductivity [Λ_M/Ω^{-1} cm^2 mol^{-1}]: 170 (in MeOH). Selected IR bands [$\tilde{\nu}$ /cm^{-1}]: 3490, 3385, 3195, 3045, 2862, 1684, 1624. UV–Vis(DMF) [λ_{max}/nm (log ε/M^{-1} cm^{-1})]: 289 (4.21).

2.2.2. Preparation of single crystals of L·H_2SO_4·H_2O, 2-acetylpyridine-aminoguanidine dihydrogensulfate monohydrate

$CuSO_4·5H_2O$ (125 mg, 0.5 mmol) was mixed with hot H_2O (2 mL) and a warm solution of L·2HCl (125 mg, 0.5 mmol) in MeOH (4 mL) was added. This mixture was slightly heated. After 3 days a mixture of mostly green microcrystals (of undefined composition) and white rod-like single crystals of L·H_2SO_4·H_2O (in a smaller quanity) were filtered and washed with MeOH. Yield of the mixture: 100 mg.

*2.2.3. [$CuLCl_2$](**1**)*

$CuCl_2·2H_2O$ (85 mg, 0.5 mmol) was mixed with hot H_2O (2 mL) and a warm solution of L·2HCl (125 mg, 0.5 mmol) in MeOH (4 mL) was added. This mixture was slightly heated. After 48 hours green crystals were filtered and washed with MeOH. Yield: 90 mg (58%). *Anal.* Calc. for $C_8H_{11}Cl_2CuN_5$: C, 30.83; H, 3.56; N, 22.47; Cl, 22.75. Found: C,

30.59; H, 3.45; N, 22.30; Cl, 22.51%. Conductivity [Λ_M/Ω^{-1} cm^2 mol^{-1}]: 27 (in DMF). Selected IR bands [$\tilde{\nu}$ /cm^{-1}]: 3392, 3251, 3181, 1645, 1607, 643. UV–Vis(DMF) [λ_{max}/nm (log ε/M^{-1} cm^{-1})]: 290 (4.02), 325 (3.87), 434 (3.60), 680 (2.23).

*2.2.4. [CuLCl$_2$](**1a**)*

Cu(OAc)$_2$·H$_2$O (100 mg, 0.5 mmol) was mixed with hot H$_2$O (2 mL) and a warm solution of L·2HCl (125 mg, 0.5 mmol) in MeOH (4 mL) was added. This mixture was slightly heated. After 48 hours green crystals were filtered and washed with MeOH. Yield: 85 mg (55%). *Anal.* Calc. for $C_8H_{11}Cl_2CuN_5$: C, 30.83; H, 3.56; N, 22.47; Cl, 22.75. Found: C, 30.65; H, 3.65; N, 22.39; Cl, 22.38%.

*2.2.5. [CuL(Cl)MeOH]NO$_3$ (**2**)*

Cu(NO$_3$)$_2$·3H$_2$O (121 mg, 0.5 mmol) was mixed with hot H$_2$O (2 mL) and a warm solution of L·2HCl (125 mg, 0.5 mmol) in MeOH (4 mL) was added. This mixture was slightly heated. After 48 hours green crystals were filtered and washed with MeOH. Yield: 55 mg (30%). *Anal.* Calc. for $C_9H_{15}ClCuN_6O_4$: C, 29.19; H, 4.08; N, 22.70; Cl, 9.57. Found: C, 29.02; H, 4.00; N, 22.51; Cl, 9.32%. Conductivity [Λ_M/Ω^{-1} cm^2 mol^{-1}]: 76 (in DMF). Selected IR bands [$\tilde{\nu}$ /cm^{-1}]: 3400, 3263, 3179, 1645, 1606, 1384, 643. UV–Vis(DMF) [λ_{max}/nm (log ε/M^{-1} cm^{-1})]: 290 (3.94), 324 (3.94), 430 (3.30), 681 (1.93).

*2.2.6. (CuL(Cl)Br)(**3**)*

CuBr$_2$ (110 mg, 0.5 mmol) was mixed with hot H$_2$O (2 mL) and a warm solution of L·2HCl (125 mg, 0.5 mmol) in MeOH (4 mL) was added. This mixture was slightly heated. After 24 hours green crystals were filtered and washed with MeOH. Yield: 95 mg (53%). *Anal.* Calc. for $C_8H_{11}ClBrCuN_5$: C, 26.98; H, 3.11; N, 19.67. Found: C, 27.12; H, 3.06; N, 20.09%. Conductivity [Λ_M/Ω^{-1} cm^2 mol^{-1}]: 57 (in DMF). Selected IR bands [$\tilde{\nu}$ /cm^{-1}]: 3394, 3250, 3179, 1645, 1608, 644. UV–Vis(DMF) [λ_{max}/nm (log ε/M^{-1} cm^{-1})]: 291 (3.92), 325 (3.89), 433 (3.30), 674 (1.80).

*2.2.7. [CuL(NCS)Cl](**4**)* and *[CuL(NCS)(SCN)](**5**)*

Cu(OAc)$_2$·H$_2$O (100 mg, 0.5 mmol) was mixed with hot H$_2$O (2 mL) and a warm solution of L·2HCl (125 mg, 0.5 mmol) in MeOH (4 mL) and NH$_4$NCS (76 mg, 1 mmol) were added. The mixture was slightly heated. After 2 hours a few green single crystals were isolated (complex **4**) from the green solution, then the solution was left at the room temperature. After 24 h blue-green crystals (complex **5**) were filtered and washed with MeOH. Yield (complex **5**): 145 mg (81%). *Anal.* Calc. for $C_{10}H_{11}CuN_7S_2$ (complex **5**): C, 33.64; H, 3.08; N, 27.47; S, 17.96. Found: C, 33.00; H, 2.91; N, 26.59; S, 17.11%. Conductivity [Λ_M/Ω^{-1} cm^2 mol^{-1}]: 71 (in DMF). Selected IR bands [$\tilde{\nu}$ /cm^{-1}]: 3389, 3259, 3149, 2099, 2056, 1650, 1600, 648. UV–Vis(DMF) [λ_{max}/nm (log ε/M^{-1} cm^{-1})]: 290 (3.88), 325 (3.89), 425 (3.11), 655 (2.01).

2.3. Single-crystal X-ray crystallography

Diffraction data were collected on a Gemini S diffractometer (Oxford Diffraction), equipped with a Mo *Kα* radiation source (λ = 0.71073 Å) and a Sapphire CCD detector. Crystal screening, strategy calculations, data collection and data reduction were performed with *CrysAlisPRO* [20]. The crystal structures were solved with *SHELXT* [21], and refined by *SHELXL*-2014 [22]. *SHELXLE* [23] was used as a graphical user interface for the refinement procedures. All non-hydrogen atoms were refined anisotropically. Hydrogen atoms attached to carbon atoms were placed in ideal positions, and were refined using the riding model.

Their U_{iso} values were approximated by the U_{eq} values of their carrier atoms. The positions of the hydrogen atoms attached to the nitrogen and oxygen atoms were determined by difference Fourier syntheses, and these atoms were refined using distance restraints. Their U_{iso} values were approximated by U_{eq} values of their carrier atoms. The structures were validated with *PLATON* [24] and by extensive use of *Mercury CSD* 2016 [25] and the Cambridge Crystallographic Database (CSD) [13].

The diffraction pattern and crystal lattice of **2** displayed apparent tetragonal symmetry. Careful examination of the complete diffraction data revealed typical signs of a pseudo-merohedrally twined crystal: high R_{int} values for an apparent tetragonal *P* lattice, and a low R_{int} value for three possible monoclinic *P* lattices; the crystal structure could not be solved in tetragonal space groups. The monoclinic *P* lattice was selected and the $P2_1/c$ space group was chosen for the structure solution. The solution was successfully obtained by *SIR92* [26]. Data were passed to *PLATON* and checked for possible twin laws using the *TWINROTMAT* routine. It yielded (1 0 0 / 0 −1 0 / 0 0 −1) as the twin matrix with ca. 39% contribution of the minor domain. The refinement was completed with *SHELXL*-2014 by incorporating the found twin law and refining the twin domain ratio using TWIN/BASF commands.

Several examined crystals of L·2HCl were non-merohedrally twined. This could be easily seen by examination of the diffraction frames during crystal screening, which clearly showed splitting of the reflections. Since no untwined specimen was found, diffraction data for a twined crystal were collected. The observed diffraction maxima were successfully indexed by two independently oriented, but identical lattices. Their mutual orientation (the twin law) was determined with *CrysAlisPRO*. Simultaneous integration of reflections belonging to both domains was performed and the domain ratio was determined by deconvolution of the intensities of partially overlapped reflections. In total, 9398 composite observations were collected (2779 fully isolated, 6619 overlapped). Reduced data were prepared for the structure solution by selecting 7548 reflections belonging to domain 1, 6169 of which represented reflections with an overlapping factor < 0.657 (chosen so that the data completeness was 80 %). After successful solution using *SHELXT*, a full dataset (3716 unique reflections), containing both isolated and overlapped reflections of both domains (HKLF5), was used for the structure refinement with *SHELXL*-2014 using the BASF command for twin domain ratio refinement. A summary of the crystallographic data for the crystal structures is given in Table 1.

2.4. Powder X-ray diffraction

Powder X-ray diffraction was performed on a Rigaku MiniFlex diffractometer, using Cu*Kα* radiation. A scan speed of 2 s per 0.03° sample rotation was used. Phase identification was performed with the program Match (Crystal Impact), using simulated powder diffractograms calculated from single crystal data.

2.5. Statistical calculations

Calculations of r.m.s. fitting and r.m.s.d. were performed with *Mercury CSD*, using the *Molecule Overlay* feature. Half-normal probability calculations included three independent pairwise comparisons of molecular geometries. For a molecule comprised of *N* atoms, 3*N*−6 independent distances were calculated [27,28]. Differences Δp_i between pairs of independent distances in the two sets, $d(1)_i$ and $d(2)_i$ are examined in a half-normal probability plot [29]. The statistic δm_i of the *i*-th parameter is calculated by eq. (1), where the quantities $d(1)_i$ and $d(2)_i$ are independent inter-atomic distances for two different structures (1) and (2) with s.u.'s $\sigma(d(1)_i)$ and $\sigma(d(2)_i)$, respectively. The experimental values δm_i are

arranged as ordered statistics and plotted *versus* the expected values (α_i) for half-normal probability deviates (tabulated in the International Tables for X-ray crystallography) [30]. The obtained plot was examined by regression analysis.

$$\delta m_i = \frac{\Delta p_i}{\sigma(\Delta p_i)} = \frac{\left|d(1)_i - d(2)_i\right|}{\sqrt{\sigma^2(d(1)_i) + \sigma^2(d(2)_i)}} \qquad (1)$$

2.6. Antimicrobial activity

The agar diffusion method was applied for susceptibility testing against standard bacterial strains: *Klebsiella pneumoniae* ATCC 29665; *Escherichia coli* ATCC 25922; *Staphylococcus aureus* ATCC 25923; *Bacillus subtilis* ATCC 6633; *Bacillus cereus* ATCC 14579 and *Micrococcus lysodeikticus* ATCC 4698, as well as for antifungal activity testing against yeast *Candida albicans* ATCC 24433. The bacterial and yeast species were cultivated on nutrient agar slants of LAB 8 and a maltose agar slant of LAB 37 (Lab M, Bury, United Kingdom), respectively. The bacteria were thermostated at 37 °C for 24 h, whilst *C. albicans* was thermostated at 28 °C for 48 h. Each grown culture was suspended in 3 mL of sterile physiological solution (8 g NaCl/L) and 0.5 mL of the suspension was carefully mixed with 10 mL of the cooled molten agar medium. In the solidified inoculated agar plates, the Ø 10 mm holes were made with sterile cork borer and 100 µL aliquots of the investigated solutions were introduced therein. After 3 h at room temperature (to permit diffusion prior to intensive microbial growth) the agar plates were thermostated as described. The obtained zones of inhibition (bactericidal and bacteriostatic) were measured. Equimolar stock solutions of the investigated complexes (5 x 10^{-2} mol/L) were prepared by dissolving in sterile deionized water with the exception of complex **4**, which was dissolved in a mixture of DMSO:H_2O = 3:2. Investigated solutions of lower concentrations (1 x 10^{-2}, 5 x 10^{-3}, 1 s 10^{-3} and 5 x 10^{-4} mol/L) were obtained by further dilution with sterile deionized water. The aqueous solutions of the ligand and Cu(II)-chloride were also tested using the described procedure.

For the samples that showed certain antimicrobial activity, the minimal inhibitory concentrations (MIC) were also determined by the agar diffusion method. Therefore, a series of five solutions in the range between the last active and the first inactive concentrations was examined.

The antifungal activity towards two strains of moulds, *Aspergillus niger* ATCC 12066 and *Aspergillus flavus sp.*[2], was investigated using a modified poisoned food technique [31]. Moulds were cultivated on a maltose agar plate at 28 °C for 4 days. Definite amounts of the investigated substances were dissolved in 5 mL of molten maltose agar by vortexing in a test tube and the prepared mediums were poured out in small Petri dishes Ø 5 cm. After medium solidification, small round cuttings of agar (Ø 5 mm) with well grown moulds were placed upsidedown on their surface and kept in a thermostat at an optimal temperature for 96 h. The diameters of the mould colonies were measured and the percent of growth inhibition was calculated by eq. (2), where *I* stands for the inhibition percent, *C* is the colony diameter in pure maltose medium as a control and *T* is the colony diameter in the tested poisoned medium.

$$I = \frac{C - T}{C} \cdot 100 \qquad (2)$$

All tests were made in duplicate and average values are presented.

[2] Strain No. 4008/2 in the collection of "Maize Research Institute Zemun Polje", Belgrade, Serbia.

3. Results and discussion

3.1. Syntheses and characterization

The Cu(II) complexes **1**-**3** were obtained in the reaction of a warm aqueous solution of the appropriate Cu(II) salt and a methanolic solution of L·2HCl in a molar ratio of 1:1. For the syntheses of **4** and **5**, NH_4NCS was added. Since it is possible that both synthetic procedures described in 2.2.3. and 2.2.4. yield a mixture of polymorphs **1** and **1a**, powder X-ray diffraction was used to identify the phase composition of the batches. The obtained experimental diffractograms, together with simulated ones (from determined crystal structures by single crystal X-ray diffraction) are shown in the Supplementary Material Figs. S1 and S2. Based on this data, it can be concluded that pure polymorph **1** is produced in the reaction of HL with $CuCl_2·2H_2O$, whereas the reaction of $Cu(OAc)_2·H_2O$ with HL leads to a mixture of polymorphs **1** and **1a**.

The attempt to synthesise the sulfato complex, by the reaction of $CuSO_4$ and L·2HCl under the same experimental conditions, resulted in the formation of a mixture of green microcrystals (of undefined composition) and white rod-like single crystals of the sulfate salt of the ligand, $L·H_2SO_4·H_2O$.

The complexes and ligands are stable in air. All the complexes are well soluble in DMF, and sparingly soluble in MeOH and EtOH.

The molar conductivity of a DMF solution of complex **2** is in accordance with its proposed coordination formula (*i.e.* a 1:1 type of electrolyte), while the conductivities of **1**, **3** and **5** have higher values than expected for non-electrolytes, which implies the substitution of the coligands with DMF molecules. This is especially pronounced for complexes **3** and **5** [32].

3.2. IR and electronic spectra

In these complexes, the ligand is coordinated in its neutral form, in a tridentate N_3 mode, *via* the pyridine, azomethine and imino nitrogen atoms of the aminoguanidine moiety, which was shown by single-crystal X-ray analysis (*vide infra*). However, this kind of ligand coordination is indicated by the shifts of the corresponding IR bands in the spectra of the complexes with respect to those in the spectrum of the free ligand.

Upon coordination, the strong band belonging to ν(C=N) vibrations of the azomethine group in spectra of the complexes is found in a lower energy region (ca. 1645 cm^{-1}) compared to its position in the spectrum of the ligand (1684 cm^{-1}) [11,14,33]. The band that may be ascribed to the vibrations of the guanido group appears at 1624 cm^{-1} in the ligand spectrum, but in the spectra of all the complexes it shows a negative shift of ~20 cm^{-1} [11,12].

The pyridine nitrogen coordination is indicated by a weak band, which corresponds to the bending vibration of the *py* ring, and which can be found at 645 ± 3 cm^{-1} in the spectra of the complexes [34]. In the spectrum of the free ligand, as a result of nitrogen atom protonation, broad $\nu(NH^+)$ bands of low intensity at 3100-2800 cm^{-1} are present [35,36].

Finally, in the IR spectra of complexes **2** and **5** some additional bands are present. In the spectrum of complex **2**, a very strong band attributed to $\nu(NO_3)$ vibrations is present at 1384 cm^{-1}, while the spectrum of complex **5** contains a doublet band at 2099 and 2056 cm^{-1}, which can be assigned to ν(CN) vibrations of thiocyanato ligand coordinated through the S and N atoms, respectively [34].

The electronic spectra are recorded in the spectral range 270-1000 nm. The spectrum of the ligand consists of one sharp band at 289 nm, which in the spectra of complexes is only slightly moved to lower energies upon coordination (by 1-2 nm). This band can be ascribed to strong intraligand $\pi \rightarrow \pi^*$ absorptions.

In the spectra of the complexes there are two other strong bands at ~325 and ~430 nm which are due to charge transfers and one weak band at 655-681 nm, which can be ascribed to *d–d* transitions. The differences in the positions of the *d-d* bands are the consequence of both the coordinated anions and the distortion of square-pyramidal surroundings.

3.3. Crystal structures

The dichloride and sulfate salts of the ligand were isolated in the form of single crystals, thus we were able to collect the first structural data for this Schiff base. The asymmetric unit of L·2HCl consists of the ligand molecule, protonated at the nitrogen atoms of the *py* moiety and imino group of the AG fragment, and two chloride anions (Fig. 1a). The same cation of the ligand, along with the sulfate anion and one water molecule, is contained in the asymmetric unit of $L{\cdot}H_2SO_4{\cdot}H_2O$ (Fig. 1b). The value of the C3–N5–C7 angle is in accordance with N5 protonation, which is larger than 120° (123.9(3)° for L·2HCl and 122.9(2)° for $L{\cdot}H_2SO_4{\cdot}H_2O$). In both structures the ligand cation is almost planar, with the maximum deviations from the plane being for atoms C8 (0.081 Å, for L·2HCl) and N1 (0.106 Å, for $L{\cdot}H_2SO_4{\cdot}H_2O$). As a result of delocalization, the C1–N1, C1–N2 and C1–N4 bonds are shorter than a single bond, but longer than a double bond, whilst the C2–N3 bond length has a value characteristic for a localized double bond (Table 2).

The mlecular structures of the structurally characterized complexes are shown in Fig. 2. In complexes **1**, **1a**, **2**, **4** and **5**, the Cu(II) ion is situated in a moderately or severely distorted square-pyramidal surrounding (Fig. 2). The distortion from an ideal geometry is described by the τ_5 parameter [37], which has the lowest value for the structure of complex **1** and the highest for complex **5** (Table 2). Precisely, the Cu(II) environment in complex **5** should be described as distorted square-planar, based on a four-coordinate geometry index τ_4 [38], which amounts 0.18(1). Yet, due to the presence of the thiocyanate anion in the apical position. which allows bonding with the metal ion, this structure should be considered as quasi square-pyramidal (4+1).

In all the described complexes, the chelate ligand is coordinated in a neutral form in a tridentate N_3 manner, *via* the pyridine (N5), azomethine (N3) and imino (N1) nitrogen atoms of the aminoguanidine fragment, forming two fused 5-membered chelate rings. All the Cu–ligator distances are in the range 1.932(3)-2.0418(17) Å, with the bond lengths with the pyridine nitrogen atom being the longest and those with the imino nitrogen atom being the shortest, except for the structure of **5**, in which the Cu1–N3 bond is slightly shorter than the Cu1–N1 bond. The latter trend of M–ligator distances, with the bond of the azomethine nitrogen atom being shorter than that of the pyridine nitrogen atom, was noticed in the structures of Cu(II) and Co(III) complexes with a similar Schiff base ligand [39,40]. It should be mentioned that all the Cu–coligand bond lengths have the expected values, with the equatorial ligand being closer to the metal center and the axial ligand further from it.

Deprotonation of the AG residue causes shortening of the C1–N1 bond and elongation of the C1–N2 and C1–N4 bonds by ca. 0.02 Å, while coordination of the ligand leads to angular changes in the aminoguanidine moiety, visualized through shrinking of the N3–N2–C1 and N2–C1–N1 angles, and widening of the N1–C1–N4 angle (Table 2). The same behavior upon deprotonation and coordination was reported for the Schiff base of aminoguanidine and salicylaldehyde [12].

The compound $[CuLCl_2]$ was isolated in two polymorphic forms (**1** and **1a**), both in the monoclinic system and $P2_1/c$ space group. However, their crystal structures greatly differ (*vide infra*). The asymmetric unit of **2** contains two $[CuL(Cl)MeOH]^+$ cations and two NO_3^- anions arranged in a peculiar way so that $[CuL(Cl)MeOH]NO_3$ subunits are pseudo-

symmetrically related by a non-crystallographic two-fold rotation axis. Finally, taking into account that the crystal structures of L·2HCl and L·H_2SO_4·H_2O contain the same cation, $[H_2L]^{2+}$, it is possible to perform three independent pairwise comparisons of the structural similarities between chemically identical molecules/cations: (a) the $[H_2L]^{2+}$ cation in L·H_2SO_4·H_2O and L·2HCl; (b) the [$CuLCl_2$] molecule in **1** *vs.* **1a**; (c) the chemically identical but crystallographically independent cations $[CuL(Cl)MeOH]^+$ (molecule A) *vs.* $[CuL(Cl)MeOH]^+$ (molecule B) in **2**.

One way to judge the structural differences is to perform a root-mean-square fit (r.m.s. fit) which provides a single parameter (root means square deviation, r.m.s.d.) as a measure of the global structural differences [41,42]. However, a more rigorous treatment is to perform a half-normal probability plot analysis of the differences in the geometrical parameters (bond lengths, angles and torsion angles) [27,29]. Half normal probability plots can be examined by linear regression, and the obtained slope and intercept can be interpreted in following way. A linear plot with a slope of unity and a zero intercept indicates a correct match between the compared sets of distances and correctly estimated e.s.d.'s. Overestimation or underestimation of the e.s.d.'s is indicated by slope larger or smaller than unity, respectively. On the other hand, a non-linear plot, or a linear plot with a non-zero intercept, points to systematic differences that may be caused by either geometrical differences in the compared structures or by systematic errors in the measurement procedures. The results of these analyses are presented in Fig. 3 and Table 3.

All three probability plots show a certain degree of linearity, but also contain several points that significantly deviate from linearity. Based on the regression parameters of the linear part of the plots (Table 3) it can be concluded that the bond length e.s.d.'s are underestimated by factor of ca. 1.5–4.5 for structures compared in Figs. 3a–c. The values of the intercepts do not deviate significantly from zero in comparisons, represented by Figs. 3a and 3b, whilst a significant deviation is observed in the graph Fig. 3c. This indicates that there is a general similarity in the structures of the cation $[H_2L]^{2+}$ in L·H_2SO_4·H_2O and L·2HCl, as well as [$CuLCl_2$] in **1** and **1a**, while there are systematic differences between the structures of the two independent cations in **2**. However, several parameters deviate considerably from linearity, which means that parts of the fitted structures show statistically significant differences.

Table 4 summarizes the most disagreeable δm_i values for the corresponding interatomic distances for the structures compared by half normal probability plots. For the comparison of the [$CuLCl_2$] molecule in **1** *vs.* **1a**, the most prominent differences are in those distances involving chlorido ligands. Similarly, comparison of the $[CuL(Cl)MeOH]^+$ cations of **2**, the greatest differences are again within the copper coordination sphere, marking that part of the molecule as the most flexible.

In addition to slightly different molecular structures, as described above, the polymorphic forms **1** and **1a** show differences in their crystal structures. Since the molecular packing is mainly determined by the formed N–H···Cl hydrogen bonds, their analysis through the graph set descriptors [43] clearly describes the different packing features. It can be seen that differences exist between the first order hydrogen-bonding networks formed.

In both polymorphic forms, all potential hydrogen bond donors and acceptors are involved in hydrogen-bonding interactions. In the form **1**, the hydrogen bonds N1–H1···$Cl2^{i}$ and N4–H4*A*···$Cl1^{i}$ connect molecules into $C_1^1(4)$ motifs, while N2–H2···$Cl2^{ii}$ and N4–H4*B*···$Cl2^{ii}$ hydrogen bonds form ring patterns of the type $R_2^2(10)$ and $R_2^2(12)$, respectively (for symmetry codes see Table S1 in the Supplementary Material). In this way, hydrogen-bonded dimers are formed in the crystal structure of form **1** by two inversion related molecules. On the other hand, all hydrogen bonds present in form **1a** (Table S2 in the

Supplementary Material) connect molecules only in chain-type motifs $C_1^1(n)$, n = 4–6, so that there are no hydrogen-bonded dimers encountered in form **1a**. Depictions of the hydrogen-bonding motifs are shown in Figs. S3 and S4 in the Supplementary Material.

3.4. Antimicrobial activity

As supposed, the synthesized compounds (2-acetylpyridine-aminoguanidine dihydrogenchloride, L·2HCl, and its complexes with Cu(II), **1**-**3** and **5**) showed antimicrobial effects, but only moderate to low on bacterial and low to missing on some fungal species. However, it was established that the Cu^{2+} ion itself had certain activity at higher concentrations.

The minimal inhibitory concentration (MIC), *i.e.* the substance concentration that totally inhibits growth of certain microorganism, is taken as a measure of the antibacterial activity. The obtained MIC values for the applied bacterial strains are given in Table 5. Those were average values of the last concentrations in the series giving bactericidal zones (totally clear agar). Often, bacteriostatic zones (with partially inhibited growth) were observed at lower concentrations.

It is noticeable that the complexes are more active compared with the metal ion itself and especially the free ligand, while the antibacterial activity is practically independent of the other residues in the complex structure. The established MIC values for the ligand are in the range 1.5 x 10^{-2} mol/L (3.75 g/L) for *B. cereus* to 3.0 x 10^{-2} mol/L (7.50 g/L) for *M. lysodeikticus*; in most cases (*K. pneumoniae*, *E. coli*, *S. aureus*, *B. subtilis*) the value 2.0 x 10^{-2} mol/L (5.00g/L) is obtained. The complexes were 11-36 times more active than the ligand (11 times for *K. pneumoniae*, 25 times for *E. coli* and *S. aureus*, 22 times for *B. subtilis*, 18 times for *B. cereus* and 36 times for *M. lysodeikticus*), which is on average ca. a twenty times higher antibacterial activity. Therefore, it could be concluded that the crucial factors for antibacterial activity of the complexes are: presence of copper, thermodynamic stability in aqueous solutions and enhanced transport through cell walls in comparison to the free metal ion. Due to their inclusion in the metabolic processes, the homeostasis of copper in the bacterial cell is disturbed.

The susceptibility of the bacterial strains applied was different toward the Cu^{2+} ion and the investigated complexes as well. For most of the strains (*E. coli, S. aureus, B. subtilis, B. cereus*) the MIC values for the complexes (which were 44.5-63.5 mg/L calculated as Cu) were approximately three times lower in comparison to the values obtained for the Cu^{2+} ion itself (158.9 mg/L). For *K. pneumoniae*, the MIC values were higher than for other bacteria (111.2 mg/L on average for the complexes, 190.6 mg/L for the Cu^{2+} ion) and the complex activity was on average only 1.9 times higher than for the free copper ion. The latter is in accordance with the fact that some strains of this bacterial species are extremely resistant to high copper concentrations [44,45]. The biggest change in susceptibility caused by copper complexation with 2-acetylpyridine-aminoguanidine was shown for the strain *M. lysodeikticus*: from 254.2 mg/L for the Cu(II) ion to an average of 53.2 mg Cu/L for the complexes, that means an increased susceptibility of 4.8 times.

None of the investigated compounds showed antifungal activity toward *C. albicans*. That is in accordance with the fact that yeasts, especially *C. albicans,* are more resistant to

high concentrations of copper than other species [46,47]. On the other hand, it is well known that Cu(II) ions inhibit mould growing [48-50]. The mechanism of action includes strong Cu^{2+} bonding with the amino groups of chitin and chitosane of the mould cell walls, wherein their normal growth is interrupted [51]. Due to the conclusion that the antibacterial activity of the synthesized complexes was independent of fine structural differences, the antifungal activity towards moulds was investigated only for complex **2**, the free ligand 2-acetylpyridine-aminoguanidine and copper(II) chloride in a concentration of 5×10^{-3} mol/L of maltose agar. The obtained results are given in Table 6. It can be seen that the ligand is not active, and contrary to its antibacterial activity, the complex inhibits mould growth almost two times weaker than the copper ion itself. The weaker activity of the complex could be explained by its high thermodynamic stability in aqueous solutions and therefore low concentration of the free Cu^{2+} ion. The applied *A. flavus* strain was more susceptible to copper than the *A. niger* strain.

4. Conclusions

Dichloride and sulfate salts of the ligand 2-acetylpyridine-aminoguanidine were isolated in the form of single crystals, thus the first structural data on this ligand are described. Besides, the first series of its Cu(II) complexes was synthesized. X-ray analysis showed the tridentate N_3 manner of chelate ligand coordination, *via* pyridine, azomethine and imino nitrogen atoms of the aminoguanidine fragment. In complexes **1**, **2**, **4** and **5**, the Cu(II) ion is situated in a moderately or severely distorted square-pyramidal surroundings. The synthesized ligand 2-acetylpyridine-aminoguanidine showed a low antimicrobial activity only toward the investigated bacterial strains. It was not active against yeast and moulds strains. The copper(II) complexes with this ligand were moderately active toward bacteria and slightly toward moulds. The antimicrobial activity of these complexes could be attributed to the presence of a copper(II) ion in the thermodynamically stable structure. The observed differences among the distinct species could be explained by different mechanisms and sites of copper action, depending on the cell wall structure and cell metabolism.

Supplementary data

CCDC 1460837-1460843 contain the supplementary crystallographic data for this paper. These data can be obtained free of charge from The Cambridge Crystallographic Data Centre via https://summary.ccdc.cam.ac.uk/structure-summary-form.

Acknowledgments

The research was supported by the Ministry of Education and Science of the Republic of Serbia (Grant no. 172014).

The *A. flavus* strain was obtained with the kindness of Dr. Jelena Lević, for which we are grateful.

References

1. C.M. da Silva, D.L. da Silva, L.V. Modolo, R.B. Alves, M.A. de Resende, C.V.B. Martins, Â. de Fátima, J. Adv. Res. 2 (2011) 1.
2. S.K. Bharti, G. Nath, R. Tilak, S.K. Singh, Eur. J. Med. Chem. 45 (2010) 651.
3. P.M. Ronad, M.N. Noolvi, S. Sapkal, S. Dharbhamulla, V.S. Maddi, Eur. J. Med. Chem. 45 (2010) 85.
4. Z.H. Huang, Z.L. Lin, J.L. Huang, Eur. J. Med. Chem. 36 (2001) 863.
5. D. Edelstein, M. Brownlee, Diabetes 41 (1992) 26.
6. I. Gardiano, A.K. Fard, D.L. Hatchell, M. Brownlee, Diabetes 47 (1998) 1114.
7. S.H. Ihm, J.H. Yoo, S.W. Park, J. Ihm, Metabolism 48 (1999) 1141.
8. T. Taguchi, M. Sugiura, Y. Hamada, I. Miwa, Eur. J. Pharmacol. 378 (1999) 283.
9. T. Taguchi, M. Sugiura, Y. Hamada, I. Miwa, Biochem. Pharmacol. 55 (1998) 1667.
10. H. Miyoshi, T. Taguchi, M. Sugiura, M. Takeuchi, K. Yanagisawa, Y. Watanable, I. Miwa, Z. Makita, T. Koike, Horm. Metab. Res. 34 (2002) 371.
11. V.M. Leovac, M.D. Joksović, V. Divjaković, Lj.S. Jovanović, Ž. Šaranović, A. Pevec, J. Inorg. Biochem. 101 (2007) 1094.
12. Lj.S. Vojinović-Ješić, M.M. Radanović, M.V. Rodić, Lj.S. Jovanović, V.I. Češljević, M.D. Joksović, Polyhedron 80 (2014) 96.
13. F.H. Allen, Acta Crystallogr., B58 (2002) 380.
14. M.M. Lalović, Lj.S. Vojinović-Ješić, Lj.S. Jovanović, V.M. Leovac, V.I. Češljević, V. Divjaković, Inorg. Chim. Acta 388 (2012) 157.
15. E.B. Shamuratov, Kh.T. Sharipov, A.S. Batsanov, Yu.T. Struchov, A.V. Khudoyarov, F.F. Mirdzhalalov, Koord. Khim. 19 (1993) 155.
16. Yu.M. Chumakov, V.I. Tsapkov, G. Bocelli, B.Ya. Antosyak, S.G. Shova, A.P. Gulea, Crystallogr. Rep. 51 (2006) 60.
17. E. A. Buvaylo, V. N. Kokozay, O. Yu. Vassilyeva, B. W. Skelton, Acta Crtystallogr. E69 (2013) m165.
18. Z. Györgydeák, W. Holzer, K. Mereiter, Monatsh. Chem 130 (1999) 899.
19. W. Schoeniger, Mikrochim. Acta 123 (1955)
20. *CrysAlisPRO* Software system, Agilent Technologies UK Ltd., Oxford, 2014.
21. G.M. Sheldrick, Acta Crystallogr., Sect. A 71 (2015) 3.
22. G.M. Sheldrick, Acta Crystallogr., Sect. C 71 (2015) 3.
23. C.B. Hübschle, G.M. Sheldrick, B. Dittrich, J. Appl. Cryst. 44 (2011) 1281–1284.
24. A.L. Spek, Acta Crystallogr., Sect. D 65 (2009)148.
25. C.F. Macrae, I.J. Bruno, J.A. Chisholm, P.R. Edgington, P. McCabe, E. Pidcock, L. Rodriguez-Monge, R. Taylor, J. van de Streek, P.A. Wood, J. Appl. Crystallogr. 41 (2008) 466.

26. A. Altomare, G. Cascarano, C. Giacovazzo, A. Gualardi, J. Appl. Cryst. 26 (1993) 343.
27. W.H. De Camp, Acta Crystallogr. Sect. A 29 (1973) 148.
28. J.D. Dunitz, X-ray Analysis and the Structure of Organic Molecules, Verlag Helvetica Chimica Acta, Basel, Switzerland, 1995, pp. 418.
29. S.C. Abrahams, E.T. Keve, Acta Crystallogr. Sect. A 27 (1971) 157.
30. W.C. Hamilton, International Tables for X-ray Crystallography, vol. IV, Kynoch Press, Birmingham, United Kingdom, 1974, pp. 293.
31. V. Kumar, D. Tyagi, J. Curr. Microbiol. App. Sci 2 (2013) 69.
32. W.J. Geary, Coord. Chem. Rev. 7 (1971) 81.
33. V.M. Leovac, Lj.S. Vojinović-Ješić, V.I. Češljević, S.B. Novaković, G.A. Bogdanović, Acta Crystallogr., C65 (2009) m337.
34. K. Nakamoto, Infrared and Raman Spectra of Inorganic and Coordination Compounds Part B, Wiley, Hoboken, New Jersey, 2009.
35. Lj.S. Vojinović-Ješić, Lj.S. Jovanović, V.M. Leovac, M.M. Radanović, M.V. Rodić, B. Barta Holló, K. Mészáros Szécsényi, S.A. Ivković, Polyhedron 101 (2015) 196.
36. M. Belicchi-Ferrari, G.F. Gasparri, E. Leporati, C. Pelizzi, P. Tarasconi, G. Tosi, J. Chem. Soc., Dalton Trans. (1986) 2455.
37. A.W. Addison, T.N. Rao, J. Reedijk, J. van Rijn, G.C. Verschoor, J. Chem. Soc., Dalton Trans. (1984) 1349.
38. L. Yang, D.R. Powell, R.P. Houser, Dalton Trans. (2007) 955.
39. V.M. Leovac, M.V. Rodić, Lj.S. Jovanović, M.D. Joksović, T. Stanojković, M. Vujčić, D. Sladić, V. Marković, Lj.S. Vojinović-Ješić, Eur. J. Inorg. Chem. (2015) 882.
40. M.V. Rodić, V.M. Leovac, Lj.S. Jovanović, Lj.S. Vojinović-Ješić, V. Divjaković, V.I. Češljević, Polyhedron 46 (2012) 124.
41. W. Kabsch, Acta Crystallogr., Sect. A 32 (1976) 922.
42. W. Kabsch, Acta Crystallogr., Sect. A 34 (1978) 827.
43. M.C. Etter, Acc. Chem. Res. 23 (1990) 121.
44. S. Zulfiqar, A.R. Shakoori, Gene 510 (2012) 32.
45. R. Shah, J. Patel, B.D. Prasad, P. Kumar, Journal of Pharmacy and Applied Sciences, 1 (2014) 1.
46. G. Dönmez, Z. Aksu, Process Biochem. 35 (1999) 135.
47. Z. Weissman, I. Berdicevsky, B.Z. Cavari, D. Kornitzer, PNAS 97 (2000) 3520.
48. J. Stevenson, A. Barwinska-Sendra, E. Tarrant, K.J. Waldron: Mechanism of action and applications of the antimicrobial properties of copper in Microbial pathogens and strategies for combating them: science, technology and education, A. Méndez-Vilas, Ed., Vol.1, FORMATEX 2013., p. 468.
49. D. Judet-Correia, C. Charpentier, M. Bensoussan, P. Dantigny, Lett. Appl. Microbiol. 53 (2011) 558.

50. E.O. Oziengbe, J.O.Osazee, Journal of Asian Scientific Research 2 (2012) 835.

51. C. Subramanyam, G. Venkateswerlu, S.L.N. Rao, Appl. Environ. Microbiol. 46 (1983) 585.

Table 1. Pertinent crystallographic and refinement details

	L·2HCl	**L·H_2SO_4·H_2O**	**1**	**1a**
Chemical formula	$C_8H_{13}Cl_2N_5$	$C_8H_{15}N_5O_5S$	$C_8H_{11}Cl_2CuN_5$	$C_8H_{11}Cl_2CuN_5$
M_r	250.13	293.31	311.66	311.66
Crystal system, space group	Monoclinic, $P2_1/c$	Monoclinic, $P2_1/c$	Monoclinic, $P2_1/c$	Monoclinic, $P2_1/c$
Temperature (K)	294	294	294	294
a (Å)	7.3584(10)	8.4366(3)	9.4721(8)	10.4309(3)
b (Å)	11.1063(11)	9.7082(3)	8.4649(7)	11.4503(3)
c (Å)	14.707(2)	15.6645(4)	14.5936(10)	10.0136(3)
β (°)	101.066(13)	97.889(3)	98.039(7)	99.068(3)
V (Å^3)	1179.6(3)	1270.85(7)	1158.62(16)	1181.05(5)
Z	4	4	4	4
Radiation type	Mo $K\alpha$	Mo $K\alpha$	Mo $K\alpha$	Mo $K\alpha$
μ (mm^{-1})	0.53	0.28	2.32	2.28
Crystal size (mm)	0.77 × 0.10 × 0.08	0.41 × 0.18 × 0.10	0.54 × 0.14 × 0.09	0.60 × 0.41 × 0.33
Absorption correction	Multi-scan	Analytical	Analytical	Analytical
T_{min}, T_{max}	0.943, 1	0.933, 0.975	0.467, 0.856	0.451, 0.562
No. of measured, independent and observed [$I > 2\sigma(I)$] reflections	3716, 3716, 2594	10128, 3003, 2707	8469, 2693, 2400	7996, 3214, 2789
R_{int}	0.043	0.020	0.019	0.017
$(\sin\theta/\lambda)_{max}$ (Å^{-1})	0.682	0.684	0.682	0.716
$R[F^2 > 2\sigma(F^2)]$, $wR(F^2)$, S	0.054, 0.163, 1.03	0.045, 0.123, 1.09	0.027, 0.068, 1.08	0.028, 0.069, 1.03
No. of reflections	3716	3003	2693	3214
No. of parameters	156	197	158	159
No. of restraints	6	9	4	4
$\Delta\rho_{max}$, $\Delta\rho_{min}$ (e Å^{-3})	0.63, –0.35	1.21, –0.31	0.31, –0.49	0.42, –0.32

Table 1. Pertinent crystallographic and refinement details (continued)

	2	**4**	**5**
Chemical formula	$C_9H_{15}ClCuN_6O_4$	$C_9H_{11}ClCuN_6S$	$C_{10}H_{11}CuN_7S_2$
M_r	370.26	334.29	356.92
Crystal system, space group	Monoclinic, $P2_1/c$	Monoclinic, $P2_1/c$	Monoclinic, $P2_1/n$
Temperature (K)	294	294	294
a (Å)	16.9088(4)	10.9851(2)	13.8349 (3)
b (Å)	13.2215(4)	14.2932(3)	7.40993 (14)
c (Å)	13.1619(3)	8.52994(17)	15.1739 (3)
β (°)	90.023(2)	103.072(2)	114.143 (3)
V (Å^3)	2942.47(13)	1304.60(5)	1419.49 (6)
Z	8	4	4
Radiation type	Mo $K\alpha$	Mo $K\alpha$	Mo $K\alpha$
μ (mm^{-1})	1.69	2.03	1.83
Crystal size (mm)	0.66 × 0.44 × 0.20	0.45 × 0.19 × 0.11	0.3 × 0.18 × 0.16
Absorption correction	Analytical	Analytical	Multi-scan
T_{min}, T_{max}	0.502, 0.744	0.553, 0.829	0.870, 1
No. of measured, independent and observed [$I > 2\sigma(I)$] reflections	43680, 7227, 6222	14596, 3163, 2719	16220, 3490, 2998
R_{int}	0.047	0.024	0.028
$(\sin \theta/\lambda)_{max}$ (Å^{-1})	0.683	0.684	0.684
$R[F^2 > 2\sigma(F^2)]$, $wR(F^2)$, S	0.031, 0.113, 1.20	0.033, 0.079, 1.09	0.037, 0.098, 1.11
No. of reflections	7227	3163	3490
No. of parameters	413	176	194
No. of restraints	10	4	4
$\Delta\rho_{max}$, $\Delta\rho_{min}$ (e Å^{-3})	0.55, –0.43	0.51, –0.35	0.50, –0.59

Table 2. Selected geometrical parameters (Å,°) of the ligands and complexes

	L·2HCl	L·H_2SO_4·H_2O	**1**	**1a**	**2** (Mol. A)	**2** (Mol. B)	**4**	**5**
Cu1–N1	–	–	1.946(2)	1.9605(17)	1.939(3)	1.932(3)	1.9452(18)	1.965(2)
Cu1–N3	–	–	1.9918(16)	1.9670(14)	1.983(3)	1.968(3)	1.9671(17)	1.9565(18)
Cu1–N5	–	–	2.0418(17)	2.0358(16)	1.999(3)	2.015(3)	2.0077(18)	2.0120(19)
Cu1–Cl1	–	–	2.2624(5)	2.2496(5)	2.2101(11)	2.2016(10)	2.7016(7)	–
Cu1–Cl2	–	–	2.5633(6)	2.5911(6)	–	–	–	–
Cu1–S1	–	–	–	–	–	–	–	3.0154(8)
Cu1–N6	–	–	–	–	–	–	1.9382(19)	1.912(2)
Cu1–O4	–	–	–	–	2.469(2)	2.505(2)	–	–
τ_5	–	–	0.04(1)	0.12(1)	0.20(2)	0.25(2)	0.06(1)	0.30(3)
C1–N1	1.302(5)	1.315(2)	1.290(3)	1.290(2)	1.295(5)	1.289(5)	1.292(3)	1.291(3)
C1–N2	1.354(4)	1.360(2)	1.386(2)	1.369(2)	1.380(4)	1.374(4)	1.370(3)	1.380(3)
C1–N4	1.318(5)	1.307(2)	1.330(3)	1.336(3)	1.329(5)	1.338(5)	1.342(3)	1.328(3)
N2–N3	1.364(4)	1.358(2)	1.352(3)	1.350(2)	1.352(4)	1.355(4)	1.358(2)	1.352(3)
C2–N3	1.283(4)	1.284(2)	1.288(2)	1.279(2)	1.277(4)	1.287(4)	1.276(3)	1.287(3)
N3–N2–C1	118.3(3)	117.54(15)	113.53(17)	113.66(14)	113.2(3)	113.2(3)	113.32(17)	113.36(18)
N1–C1–N4	121.4(3)	122.25(17)	127.7(2)	127.15(17)	125.7(3)	126.4(3)	125.7(2)	127.7(2)
N2–C1–N1	121.4(3)	120.56(17)	117.0(2)	117.69(17)	117.7(3)	116.9(3)	117.54(19)	117.4(2)

Table 3. Regression analysis of half-normal probability plots. The equation fitted is $\delta m_i = B\alpha_i + A$, n is the number of parameters used in regression analysis, R is the correlation coefficient. The errors indicate a 95% confidence interval.

Comparison	*n*	*B*	*A*	*R*	*r.m.s.d.* (Å)
Fig. 3a	28	1.566±0.052	–0.030±0.080	0.986	0.0468
Fig. 3b	32	4.465±0.121	–0.078±0.075	0.989	0.0731
Fig. 3c	39	2.951±0.051	–0.303±0.039	0.994	0.0580

Table 4. Most disagreeable δm_i values for the corresponding interatomic distances for the complexes compared in Fig. 3.

Fig. 3a			Fig. 3b			Fig. 3c		
δm_i	Distance	Order†	δm_i	Distance	Order†	δm_i	Distance	Order†
6.11	C3–C8	Second	52.90	N5–Cl2	Second	15.92	C9–Cl1	Third
4.30	N1–N3	Third	33.42	N1–Cl2	Second	13.52	N5–O4	Second
3.80	C7–N5	First	32.76	Cu1–Cl2	First	10.64	Cu1–O4	First
3.67	C4–C8	Third	21.07	N5–Cl1	Second	9.54	N1–O4	Second
3.67	C6–N5	Second	19.20	N1–Cl1	Second	5.72	Cu1–Cl1	First
2.25	C4–N5	Second	18.10	Cu1–Cl1	First	4.11	N1–N3	Second

† First-, second- and third-order number represents the distance between two atoms separated by one, two or three formal bonds.

Table 5. MIC x 10^3 (mol/L) of the copper(II) complexes with 2-acetylpyridine-aminoguanidine, the free metal ion and ligand

Compound	Bacterial species					
	K. pneumoniae	*E. coli*	*S. aureus*	*B. subtilis*	*B. cereus*	*M. lysodeikticus*
1	2	0.75	0.8	0.9	0.8	0.85
2	2	0.8	0.8	1	0.95	0.85
3	2	0.8	0.8	1	0.85	0.85
5	1	0.8	0.8	0.8	0.7	0.8
$CuCl_2{\cdot}2H_2O$	3	2.5	2.5	2.5	2.5	4
L·2HCl	20	20	20	20	15	30

Table 6. Inhibition % for the investigated moulds obtained with 5 x 10^{-3} mol/L solutions

Mould	Compound		
	$CuCl_2{\cdot}2H_2O$	L·2HCl	**1**
A. niger	39.5	0	20.9
A. flavus	79.2	0	45.8

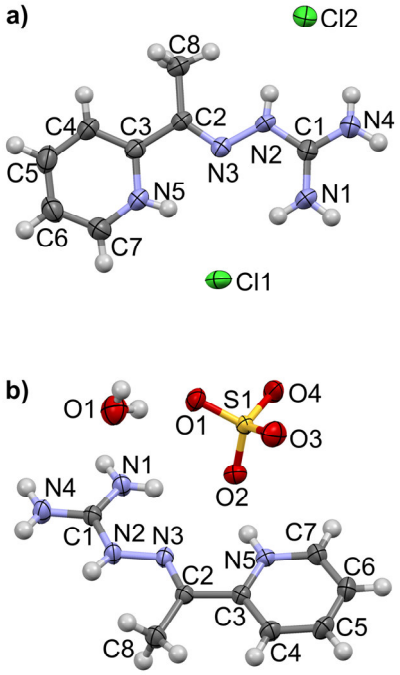

Fig. 1. Molecular structures of L·2HCl (a) and L·H_2SO_4·H_2O (b)

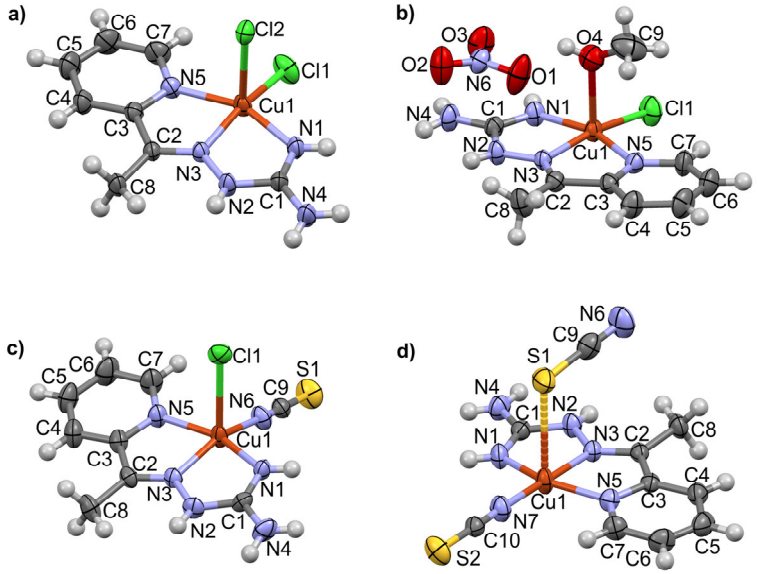

Fig. 2. Molecular structures of the complexes: a) [$CuLCl_2$] (**1**); b) [CuL(Cl)MeOH]NO_3 (**2**); c) [CuL(NCS)Cl] (**4**); d) [CuL(NCS)(SCN)] (**5**)

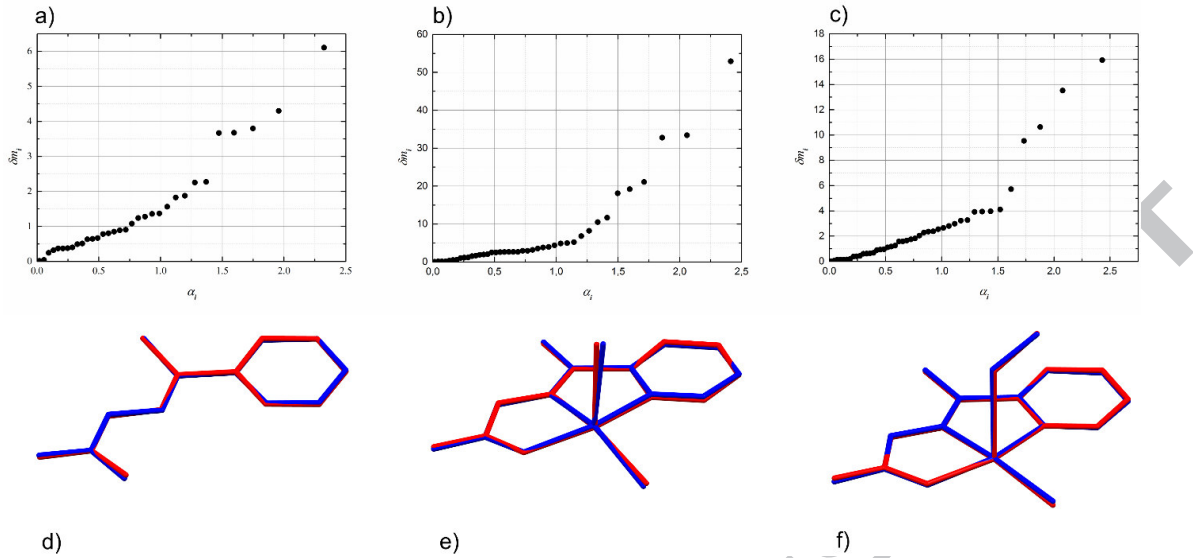

Fig. 3. Half-normal probability plots of: (a) the cation $[H_2L]^+$ in $L{\cdot}H_2SO_4{\cdot}H_2O$ and $L{\cdot}2HCl$; (b) $[CuLCl_2]$ in **1** *vs.* **1a**; (c) $[CuL(Cl)MeOH]^+$ (molecule A) *vs.* $[CuL(Cl)MeOH]^+$ (molecule B) in **2**. R.m.s. overlays of the respective molecules are represented in (d), (e), and (f).

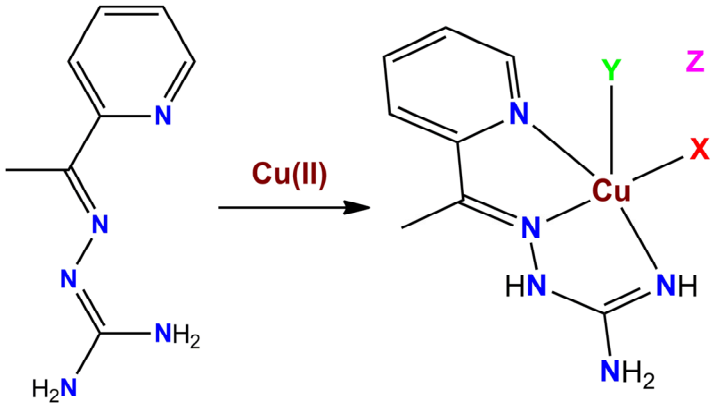

	X	Y	Z
1	Cl	Cl	/
2	Cl	MeOH	NO_3
3	Cl	Br	/
4	NCS	Cl	/
5	NCS	SCN	/

Graphical abstract

A series of five Cu(II) complexes with the tridentate N_3 ligand 2-acetylpyridine-aminoguanidine, being the first complexes with this ligands, was synthesized and characterized. Single crystal X-ray analysis showed a moderately or severely distorted square-pyramidal surroundings of the Cu(II) ion in these complexes. Additionally, the antimicrobial activity of the obtained compounds was estimated.

Synopsis